*Original research article*

ENERGY EXPLORATION & EXPLOITATION

Energy Exploration & Exploitation
1–17

DOI: 10.1177/01445987251373101
journals.sagepub.com/home/eea

Sage

# Design and real-time simulations of robust controllers for uncertain multi-input wind turbine

**NVA Ravikumar[1], Rebba Sasidhar[2], Vasupalli Manoj[1], Chandini Mutta[3], Mekala Chandra Sekhara Reddy[4], K Jagath Narayana[4], Daniel Eutyche Mbadjoun Wapet[5] and Mohamed Metwally Mahmoud[6,7]**

## Abstract

The problem of uncertainty in wind turbines is caused by factors like the random and stochastic nature of the wind, variations in the moment of inertia of its rotating parts, damping, stiffness factors, and discrepancies between its actual and mathematical model. The presence of uncertainty would deteriorate the wind turbine's performance, which can significantly affect rotor speed. Therefore, robust control strategies for speed control are necessary in the presence of uncertainties and wind disturbances, with the help of the control input taken as the blade pitch angle. Hence, a robustly stabilizing proportional-integral (PI) controller is designed under the purview of Kharitonov's polynomials to control the rotor speed for a $\pm 25\%$ uncertain multi-input wind turbine. The robustly stabilizing ($K_p$, $K_i$) region of the designed PI controller is obtained by Kharitonov's theorem based on the 16-plant model after the formation of Kharitonov's rectangles. A ($K_p$, $K_i$)-subregion is also extracted for all plants individually to achieve the desired time response specifications. The purpose of this analysis is to make sure that a simple PI controller

[1]Department of Electrical & Electronics Engineering, GMR Institute of Technology, Rajam, Andhra Pradesh, India
[2]Department of Electrical & Electronics Engineering, Avanthi Institute of Engineering and Technology, Vizianagaram, Andhra Pradesh, India
[3]Department of Electrical & Electronics Engineering, Potti Sriramulu Chalavadi Mallikharjuna Rao College of Engineering and Technology, Vijayawada, Andhra Pradesh, India
[4]Department of Mechanical Engineering, Sri Venkateswara College of Engineering, Tirupati, Andhra Pradesh, India
[5]National Advanced School of Engineering, Université de Yaoundé I, Yaoundé, Cameroon
[6]Department of Electrical Engineering, Faculty of Energy Engineering, Aswan University, Aswan, Egypt
[7]Jadara University Research Center, Jadara University, Irbid, Jordan

**Corresponding author:**
Mohamed Metwally Mahmoud, Department of Electrical Engineering, Faculty of Energy Engineering, Aswan University, Aswan, Egypt.
Email: metwally_m@aswu.edu.eg

can be made robust when there is a provision to choose its parameters from the stabilizing regions achieved. Real-time simulations are also made on the OPAL RT OP5700 Simulator to validate the performance of robust controllers designed in MATLAB. The real-time results clearly validate the performance of robustly designed controllers.

**Keywords**
Robust control, uncertainty modeling, multi-input systems, wind turbines, real-time simulations

## Introduction

A single large contemporary wind turbine (WT) may generate several megawatts, which are expensive, need regular maintenance, and must endure harsh weather conditions, primarily variations in wind speeds. The significant increase in wind energy, viz., large WT, imposes challenges to the control domain's perspective owing to the unmodelled dynamics of the WT, fatigue, aerodynamics, structural analysis, and turbulence (El Beshbichi et al., 2023), (Adeoye et al., 2024), (Metwally Mahmoud, 2023). These factors sum up to create uncertainty in the WT (Salem et al., 2017), (Mahmoud et al., 2022b), (Boudjemai et al., 2023b). A model called stochastic network-constrained unit commitment (NCUC), as introduced in the work (Naghdalian et al., 2020), has been developed. By considering the required flexible ramp and spinning reserves in the face of demand and wind power uncertainty, it seeks to determine the optimal daily plan for generating units.

Research has been carried out invariably in the control aspects of WTs (Mahmoud et al., 2023b), (Mahmoud et al., 2023a), (Boudjemai et al., 2023a), (Aldin et al., 2023). The risk of failures increases in the modern power system dynamics due to increased use of renewables, and hence, must account for frequency control to detect grid power imbalances (Kheshti et al., 2020), (Atia et al., 2024). The blade pitch control system is designed for wind systems (Mahmoud et al., 2022a), which discusses the fundamental construction of WTs, control loops, controllers, and their latest advancements. A review on the control of WTs to improve their performance based on desired objectives encompassing cost reduction, increased energy capture, and the combination of both is presented (Apata and Oyedokun, 2020). The variable speed WTs were controlled by controlling the blade pitch angle (Bahmani et al., 2020). It is used primarily under strong wind currents to limit power extraction from wind energy. Pitch control is possible in two ways: control of combined pitch and control of individual pitch. The latter is used in large WTs to restrict the output under strong winds (Hamoodi et al., 2020), (Boudjemai et al., 2025). A novel strategy using adaptive fuzzy logic is developed for improved performance of turbine-generator systems for wind energy extraction (Soliman et al., 2019), (Menzri et al., 2024).

In (Rigatos and Siano, 2011), a power system stabilizer is suggested that is built in a simulated setting using the extremal gain-margin theory of Kharitonov. It stabilizes a small number of extreme plants, which results in the design of a controller having low order and exhibiting the characteristics of a phase-lead compensator that is resistant to operating point changes. A robust controller to damp out the oscillations during the wind power generation is considered in (Isbeih et al., 2019), (Boutabba et al., 2025). An effective strategic approach known as an integral backstepping strategy (IBS) is applied on a variable-speed generator for optimal power extraction by the WT (Saidi et al., 2021). By using this control mechanism, the mechanical stress on the WT and generator shafts is reduced. A decoupled PI current controller is designed for WTs sourcing an inverter tied to the grid (Errouissi et al., 2018).

This work outlines the design of a PI controller aimed at stabilizing a range of interval plants (Matušů, 2011). Additionally, it offers a thorough evaluation of every stabilizing PI controller

appropriate for this kind of interval plant family. In (Petkov et al., 2018), the authors developed a robust controller for a model that was uncertain, which includes the design of three robust controllers, namely $H_\infty-$, $\mu$-, and loop shaping. The authors in (Bhattacharyya, 2017) delved into the topic of robust control in the presence of parametric uncertainty.

The disturbances in power quality are compensated to overcome the problem of uncertainty in renewable generation at the point of common coupling (Chishti et al., 2020). The harmonics produced due to the nonlinear component of load current are filtered by a robust, normalized, mixed-norm adaptive algorithm. A sliding mode controller for a doubly-fed induction generator-based WT was explored to regulate the speed and the generated power in the presence of uncertainties (Jafari and Shahgholian, 2017). Similarly, a second-order sliding mode controller was explored to optimize the generation of power by a WT (Liu et al., 2017). During the design of a WT model for analysis, there is a chance of neglecting the environmental conditions and working parameters (Cascianelli et al., 2022), (Huang et al., 2020) upon which the production of power by a WT depends. The potential danger to WT stability and performance under the effect of uncertainties has gained importance, and is thus the subject of this paper's examination. The control strategies for industrial wind turbines are the PID regulators (Habibi et al., 2018), (Fayz et al., 2025). By embedding a Nussbaum-type function with a novel PID-based fault-tolerant controller, a robust adaptive control scheme is developed for WTs. The Kharitonov-based PI controller, as described in (Asadi, 2018), is widely used for modeling a 16-plant model derived from a specified interval plant. This method is employed to establish a suitable stabilizing region for the values of $K_p$ and $K_i$, including their Kharitonov rectangles. Several researchers have provided in-depth insights into Kharitonov-based controllers, such as the 16-plant theorem (Toulabi et al., 2018), as well as the development of robust PID controllers (Chu and Chu, 2018), (Vo, 2018). The high-cost, large WTs with inevitable uncertainties need proper controllers; otherwise, the loss can be irreparable. Hence, the focus is typically on active management of bigger flexible WTs that are prone to uncertainties, to decrease the losses, viz., economic and structural, otherwise, it might lead to costly compensation (Wang et al., 2018). This discusses the necessity of designing a controller for a WT that incorporates uncertainty modeled using Kharitonov's polynomial, which can control the generator's speed using blade pitch angle control.

This study presents a unique control approach for a multi-input uncertain WT exposed to $\pm$25% uncertainty. The technique is centered on attaining a stabilizing area relating to a set of controller gains ($K_p$, $K_i$). It is found that the performance of the uncertain WT may be reliably stabilized with any set of gains. But to meet the desired time response specifications, sub-regions for all 16 individual plants were also achieved. The performance of the uncertain WT may be securely stabilized in the presence of wind disturbance with any combination of gains selected from the different sub-regions. Moreover, these performances of all individual controllers are validated in a real-time environment (OPAL RT OP5700) by simulating all 16 controlled plants to consolidate the robustness of controllers designed using Kharitonov's 16 plant theorem.

The paper's structure is as follows: Section 1 covers the introduction to wind energy, types of wind turbines, potential dangers to wind turbine stability and performance, uncertainties in wind turbines, and the control methods to deal with an uncertain WT. In Section 2, a linearized WT model with seven states is shown. In Section 3, a WT model under the presence of uncertainty is modeled. A PI controller is designed based on Kharitonov's polynomials, the mathematical preliminaries of which are presented in Section 4. The 16-plant model is used to illustrate the resilient controller design in Section 5, while the simulation results for the uncertain WT model are presented in Section 6. Lastly, section 7 presents the conclusions.

## WT mathematical model

This section presents the WT mathematical model, which was adapted in (Wright and Balas, 2003). It is a two-bladed, 600 kW, upwind machine having it's a rotational speed of 42 rpm. The seven-state linearized WT's state-space representation may be expressed as:

$$M\dot{x}(t) = Ax(t) + Bu(t) + \Gamma u_d(t) \tag{1}$$

$$y(t) = Cx(t) \tag{2}$$

where $M$ represents mass matrix $\in R^{7\times 7}$, $x(t)$ represents the state vector $\in R^{7\times 1}$, $A$ represents the system matrix $\in R^{7\times 7}$, and $B$ represents the input matrix $\in R^{7\times 1}$, $\Gamma$ represents the disturbance input matrix $\in R^{7\times 1}$, $C$ represents the control input gain matrix $\in R^{1\times 7}$, $u(t)$ represents the controlled input (blade pitch angle), $\beta$ and $u_d(t)$ represents the disturbance input (wind) and $y(t)$ represents the output vector.

The seven-states considered in equation (1) are namely: rotor blade displacement ($x_1(t)$), rotor blade velocity ($x_2(t)$), rotational speed of the rotor ($x_3(t)$), torsional force ($x_4(t)$), rotational speed of the generator ($x_5(t)$), tower's deflection ($x_6(t)$) and tower's velocity ($x_7(t)$). The constants $M_{ij}$, $K_{ij}$, and $C_{ij}$ represent mass-elements, stiffness-elements, and damping-elements, respectively ($i$ and $j$ take values from 1 to 7), $\zeta$ functions as a partial derivative of the aerodynamic torque of the rotor considering changes in $\beta$. $I_{\text{rot}}$ and $I_{\text{gen}}$ denote the rotor and generator's moments of inertia, while $K_d$ and $C_d$ represent the damping and stiffness components, respectively. These matrices are given below.

$$A = \begin{bmatrix} 0 & 1 & 0 & 0 & 0 & 0 & 0 \\ -K_{11} & -C_{11} & -C_{14} & 0 & 0 & -K_{17} & -C_{17} \\ -2K_{41} & -2C_{41} & \Upsilon - C_d & -1 & C_d & -K_{47} & -C_{47} \\ 0 & 0 & K_d & 0 & -K_d & 0 & 0 \\ 0 & 0 & C_d & 1 & -C_d & 0 & 0 \\ 0 & 0 & 0 & 0 & 0 & 0 & 1 \\ -2K_{71} & -2C_{71} & -C_{74} & 0 & 0 & -K_{77} & -C_{77} \end{bmatrix}$$

$$M = \begin{bmatrix} 1 & 1 & 0 & 0 & 0 & 0 & 0 \\ 0 & M_{11} & M_{14} & 0 & 0 & 0 & M_{17} \\ 0 & 2M_{41} & I_{rot} & 0 & 0 & 0 & 0 \\ 0 & 0 & 0 & 1 & 0 & 0 & 0 \\ 0 & 0 & 0 & 0 & I_{gen} & 0 & 0 \\ 0 & 0 & 0 & 0 & 0 & 1 & 0 \\ 0 & 2M_{71} & 0 & 0 & 0 & 0 & M_{77} \end{bmatrix}$$

$$C = \begin{bmatrix} 0 & 0 & 0 & 0 & 1 & 0 & 0 \end{bmatrix}$$

$$B = \begin{bmatrix} 0 & \alpha_b & 0 & 0 & 1 & 0 & 0 \end{bmatrix}^T$$

$$\Gamma = \begin{bmatrix} 0 & \beta_b & \beta & 0 & 1 & 0 & \beta_t \end{bmatrix}^T$$

The standard state space form is obtained by rewriting equations (1) and (2).

$$\dot{x}(t) = M^{-1}Ax(t) + M^{-1}Bu(t) + M^{-1}\Gamma u_d(t) \tag{3}$$

$$y(t) = Cx(t) \tag{4}$$

Equation (3) is rewritten as

$$\dot{x(t)} = \bar{A}x(t) + \bar{B}u(t) + \bar{\Gamma}u_d(t) \tag{5}$$

$$y(t) = Cx(t) \tag{6}$$

where, $\bar{A} = M^{-1}A,\ \bar{B} = M^{-1}B,\ \bar{\Gamma} = M^{-1}\Gamma,\ and\ \bar{C} = C$

## The uncertain WT model

Uncertainties are inevitable in real-time systems, and they are particularly apparent in the functioning of WTs. The uncertainty may be categorized into three types: disturbances due to fluctuations in wind speed, noise from measurement processes, and dynamic perturbations arising from variations between the plant's mathematical model and its real-time operational dynamics. Unmodeled dynamics due to high frequencies, the nonlinearities that were ignored during modeling, parameter variations in the system due to changing climatic conditions, and wear and tear factors can all cause dynamic perturbations in WTs. These factors can adversely affect the performance and stability of the control system.

As illustrated in Figure 1, the dynamic perturbations are grouped in a block and are known as the uncertainty matrix ($\Delta$). It is also represented by $\Delta(s)$ the uncertainty transfer function. Here, Gpert(s), which is defined by equation (7), represents the real dynamics of a perturbed WT (the dotted block in Figure 1).

$$Gpert(s) = G_{WT}(s) + \Delta(s) \tag{7}$$

where $G_{\mathrm{WT}}$ $(s)$ represents the nominal WT's transfer function and $\Delta(s)$ represents the structured uncertainty [3] given by equation (8)

$$\Delta = diag[\delta iai] \tag{8}$$

where $i = 1, 2, 3,\ldots$ 21 elements for which $\pm 25\%$ uncertainty is introduced, $a'\,'s$ are the elements of the system matrix, while the relative changes in these elements are represented by $\delta i$. In this paper, a robust stabilizing controller (PI) based on a 16-plant model of Kharitonov's theorem is proposed, which can control the blade pitch angle and speed of the generator of an uncertain WT for random variations in wind velocities.

## Kharitonov's theorem preliminaries

Stability analysis typically involves the Routh-Hurwitz stability test, which applies to fixed polynomials. However, when dealing with polynomials featuring uncertain coefficients, stability analysis can be effectively carried out using Kharitonov's theorem. Two main methods are used to evaluate polynomial stability, which are, for a particular polynomial or family of polynomials, by locating the roots in the left half of the s-plane, and by considering limitations on the polynomial or polynomial family, such as damping factor or settling time. All roots of the specified family of polynomials must exist inside the region, a subset in the left half of the s-plane, to guarantee stability (Asadi, 2018).

Def: The interval polynomial is a polynomial family defined by

$$P(s) = a_0 + a_1 s^1 + a_2 s^2 + \ldots\ldots\ldots\ldots + a_n s^n = \sum_{p=0}^{n} a_p s^p \tag{9}$$

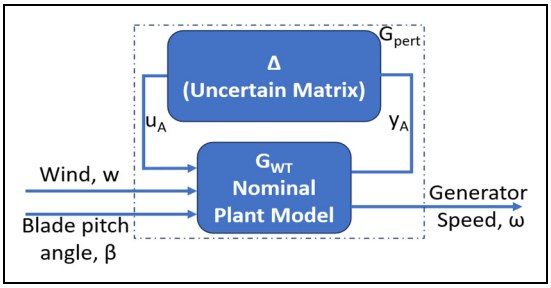


**Figure 1.** A block diagram of an uncertain wind turbine.

$\forall p$, where $a_p \in [l_p, u_p]$ and $0 \in/ [l_p, u_p]$. The boundaries (both minimum value and maximum value) of the $p^{\text{th}}$ coefficient are represented by $l_p$ and $u_p$, respectively, and the order of the polynomial $P(s)$ is denoted by $n$.

The minimum value and maximum value given by the general equation (10) yield four predefined Kharitonov's polynomials given by (Asadi, 2018), (Vo, 2018):

$$P(s, a) = \sum_{p=1}^{n} [a_p^-, a_p^+] s^p \tag{10}$$

Therefore, the fixed polynomials are expressed as equation (11).

$$\begin{aligned} K_1(s) &= a_0^- + a_1^- s^1 + a_2^+ s^2 + a_3^+ s^3 + a_4^- s^4 + a_5^- s^5 + a_6^+ s^6 + \ldots \\ K_2(s) &= a_0^+ + a_1^+ s^1 + a_2^- s^2 + a_3^- s^3 + a_4^+ s^4 + a_5^+ s^5 + a_6^- s^6 + \ldots \\ K_3(s) &= a_0^+ + a_1^- s^1 + a_2^- s^2 + a_3^+ s^3 + a_4^+ s^4 + a_5^- s^5 + a_6^- s^6 + \ldots \\ K_4(s) &= a_0^- + a_1^+ s^1 + a_2^+ s^2 + a_3^- s^3 + a_4^- s^4 + a_5^+ s^5 + a_6^+ s^6 + \ldots \end{aligned} \tag{11}$$

According to Kharitonov's Theorem, the four fixed Kharitonov polynomials must be stable in order to achieve an interval polynomial family, $P(s, a)$, that is robustly stable (Asadi, 2018).

Lemma: The following properties must be true for an $n^{th}$ order interval polynomial given by (10) to be robustly stable (Asadi, 2018). They are:

- stable $K_3(s)$ when $n = 3$
- stable $K_2(s)$ and stable $K_3(s)$ when $n = 4$
- stable $K_2(s)$, stable $K_3(s)$ and stable $K_4(s)$ when $n = 5$
- stable $K_1(s)$, stable $K_2(s)$, stable $K_3(s)$ and stable $K_4(s)$ when $n \geq 6$

## *Formation of 16 Kharitonov plants*

Upon introduction of ±25% uncertainty for the aforementioned 21 system matrix elements in Section 3, an uncertain family of polynomials is formed for both the numerator and denominator pertaining to the nominal transfer function given by equation (12).

$$P(s, a, b) = \frac{N(s, a)}{D(s, b)} = \frac{\sum_{p=0}^{m} [a_p^-, a_p^+] s^p}{s^n + \sum_{p=0}^{n-1} [b_p^-, b_p^+] s^p} \tag{12}$$

The equation (12), $P(s, a, b)$, should be proper strictly. Four Kharitonov's polynomials are then produced by the numerator and denominator polynomials, respectively. Tables 1 and 2 are formed because of the application of ±25% uncertainty, respectively, to the 21 system matrix elements, yielding lower and upper bounds.

Kharitonov's theorem introduces the 16-plant theorem, which involves obtaining Kharitonov polynomials for the numerator and denominator separately, i.e., $N_1(s)$, $N_2(s)$, $N_3(s)$ and $N_4(s)$ and $D_1(s)$, $D_2(s)$, $D_3(s)$ and $D_4(s)$ (Asadi, 2018). Hence, according to equation (13), the 16 Kharitonov plants are obtained as follows:

$$p_{i_1,i_2(s)} = \frac{N_{i_1}(s)}{D_{i_2}(s)} \tag{13}$$

where $i_1, i_2 \in 1, 2, 3, 4$

### *Kharitonov's rectangles*

A rectangle is formed from the four fixed polynomials given in equation (11) for a given value of $\omega$. The value of $\omega$ is varied in steps from 0 to $\omega_0$ to obtain a set of rectangles known as Kharitonov's rectangles. According to the zero exclusion principle (Asadi, 2018), the location of origin in the complex plane should lie out of range with the locus of rectangles, and the same is achieved as shown in Figure 2; then the four determined polynomials are said to be stable.

## The robust controller design methodology utilizing a 16-plant model

The control scheme illustrated in Figure 3 depicts a robustly stabilizing PI controller designed for an uncertain wind turbine, employing Kharitonov's theorem (16-plant model approach). The goal of this PI controller design is to stabilize all members of the polynomial family defined by $P(s, a, b)$.

### *Procedure for designing suitable gains for the controller*

The following steps are needed to develop a robust controller with suitable parameter ranges for each of the 16 plants:

- Equation (13) yields the 16 related plants.
- Selecting a first-order PI controller, denoted by the formula $C(s) = K_p + \frac{K_I}{s}$, in which the integral and proportional gain constants are denoted by $K_p$ and $K_i$, respectively.
- The allowed parameter ranges for each of the 16 plants are found using the Routh-Hurwitz table.
- Ultimately, the range of admissible controller gains $C(s)$ that can effectively stabilize the specified polynomial family is determined by intersecting these 16 inequalities.

### *Acceptable stabilizing region of the controller*

A region is obtained upon the intersection of all the 16 plant inequalities given in Section 5.1. This region can be called an acceptable stabilizing ($K_p$, $K_i$) region of the controller. Because any set of gains from this region can stabilize any plant from the 16 plants formed using Kharitonov's 16-plant theorem. Since ±25% uncertainty is also considered to model the 16 plants, this region can also be called the robustly stabilizing region of the controller gains and is shown in Figure 4. It is observed

**Table 1.** Coefficients associated with numerator polynomials.

| Coefficient term | $S^4$ | $S^3$ | $S^2$ | $S^1$ | $S^0$ |
|---|---|---|---|---|---|
| Nominal ($\overline{a_i}$) | 2.007 | 87.38 | 6897 | 3238 | 234,300 |
| Min ($a_i^-$) | 1.50525 | 65.535 | 5172.75 | 2428.5 | 175,725 |
| Max ($a_i^+$) | 2.50875 | 109.225 | 8621.25 | 4047.5 | 292,875 |

**Table 2.** Coefficients associated with denominator polynomials formed from Kharitonov's theorem.

| Coefficient term | $S^7$ | $S^6$ | $S^5$ | $S^4$ | $S^3$ | $S^2$ | $S^1$ | $S^0$ |
|---|---|---|---|---|---|---|---|---|
| Nominal ($\overline{a_i}$) | 1 | 9.319 | 750.2 | 5110 | 129,200 | 196,200 | 3,570,000 | 439,100 |
| Min ($a_i^-$) | 1 | 6.98925 | 562.65 | 3832.5 | 969,000 | 147,150 | 2,677,500 | 329,325 |
| Max ($a_i^+$) | 1 | 11.64875 | 937.75 | 6387.5 | 161,500 | 245,250 | 446,250 | 548,875 |

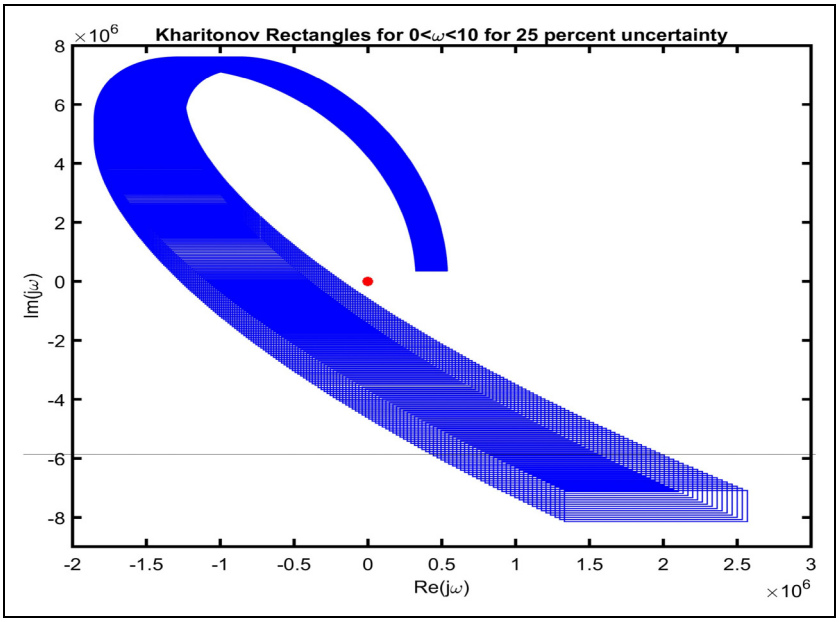


**Figure 2.** Kharitonov's rectangles validating the zero-exclusion principle. The red asterisks signify that the origin lies outside the set of rectangles, indicating stability.

that for any ($K_p$, $K_i$) pair in this allowable range stabilizes a $\pm$25% uncertain WT's performance against wind disturbances, viz., a rotor rated speed of 42 rpm.

## *Sub-regions of the controllers for each individual plant*

A sub-region is taken as the chosen portion from the acceptable stabilizing region presented in 5.2 for each individual plant. The sub-regions for each individual plant are depicted in Figure 4. It falls within the acceptable region for ($K_p$, $K_i$). These controllers gain sets can achieve the desired time response specifications, viz., peak overshoot < 5% and settling time < 5 s.

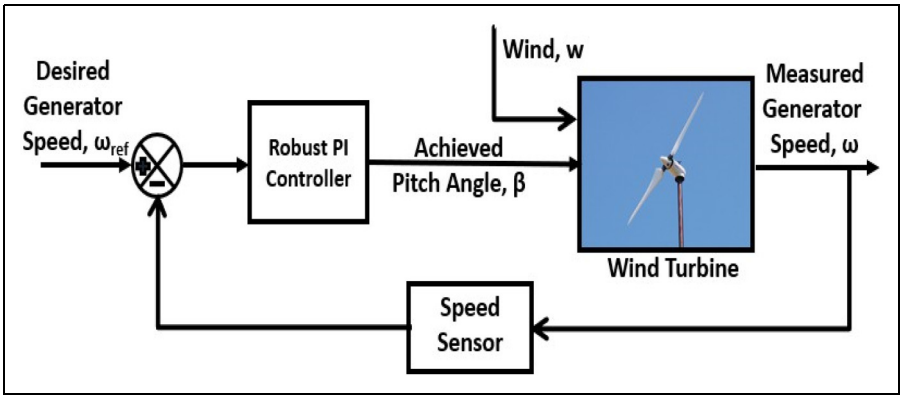


**Figure 3.** Control feedback for an interval plant $P$ ($s$, $a$, $b$).

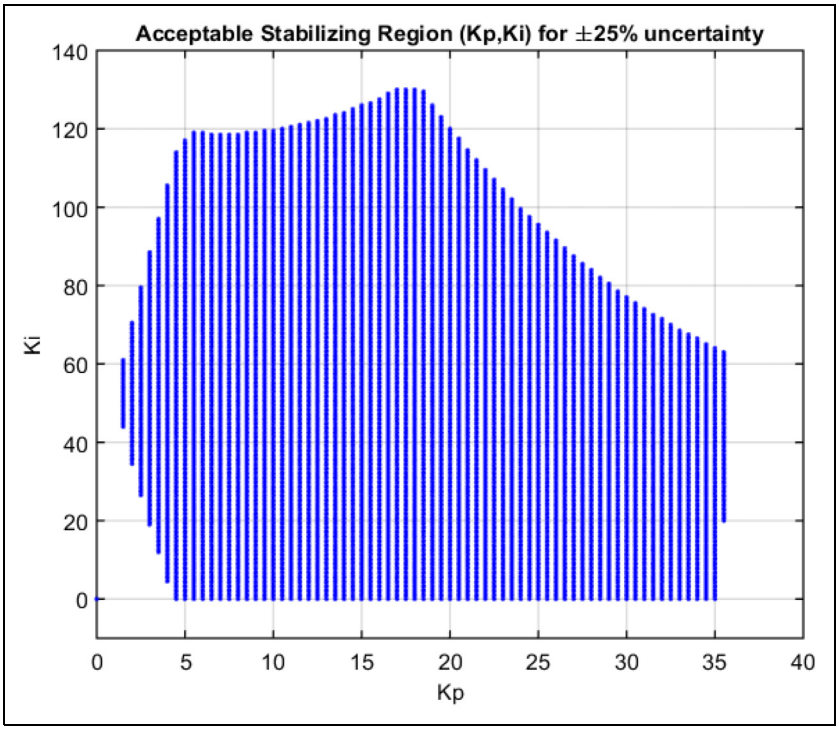


**Figure 4.** The acceptable stabilizing region for ($K_p$, $K_i$) for a $\pm$25% uncertainty being incorporated into the WT's mathematical model.

## Findings and discussions

After uncertainties were incorporated into the WT's system matrix $\bar{A}$, 150 iterations of simulations were run to ascertain the lower and upper bounds of both numerator coefficients and denominator coefficients. A seventh-order denominator and a fourth-order numerator were derived. Equation

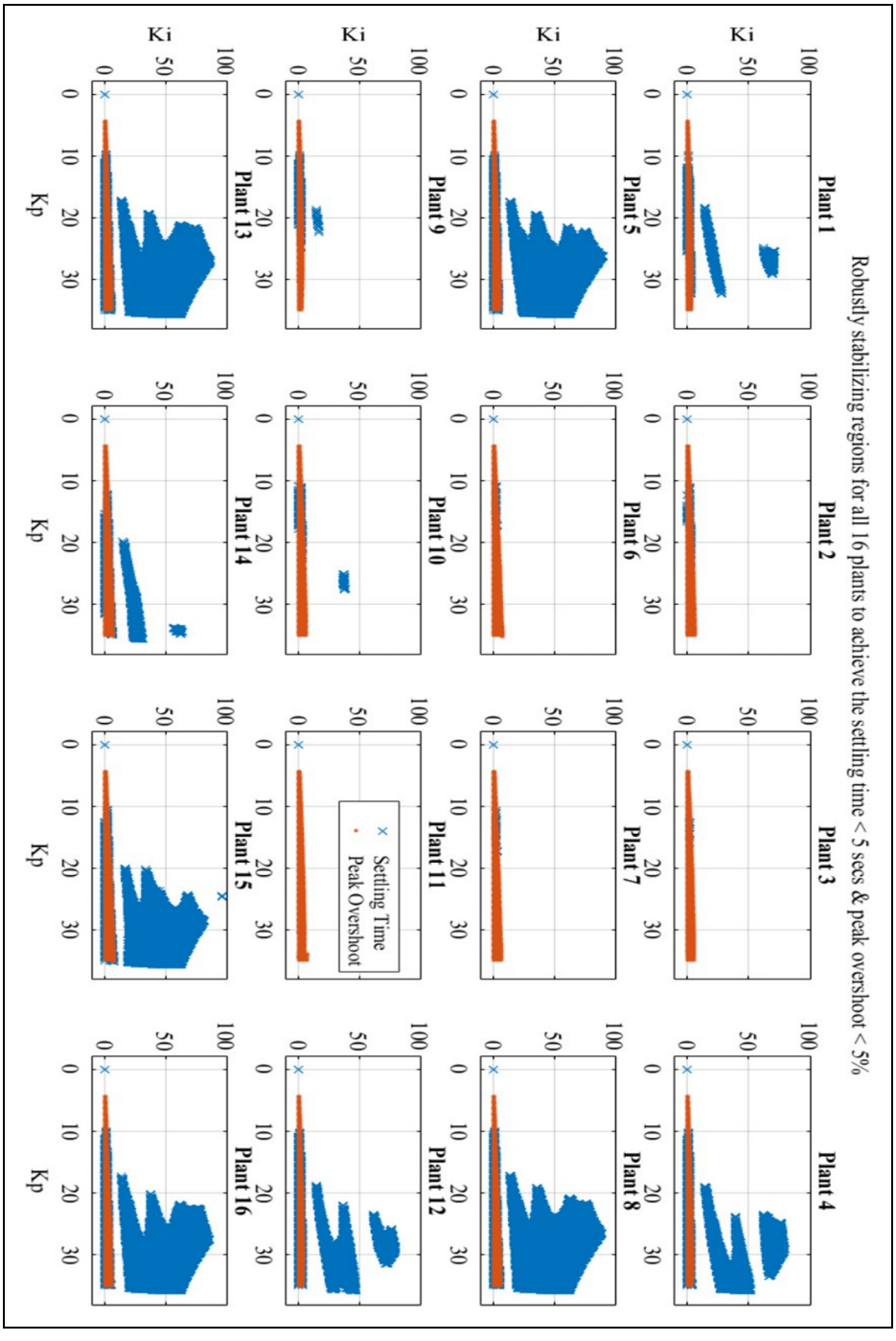


**Figure 5.** The ($K_p$, $K_i$)-subregions for all 16 plants to achieve peak overshoot < 5% and settling time < 5 s.

**Table 3.** Performance of the designed robust PI controller.

| Plant | Minimum | | Maximum | | Settling Time | | Peak Overshoot (%) | |
|---|---|---|---|---|---|---|---|---|
| | $K_p$ | $K_i$ | $K_p$ | $K_i$ | Min | Max | Min | Max |
| 1 | 10 | 0 | 32.4 | 3 | 4.81 | 4.71 | 0.463 | 4.25 |
| 2 | 11 | 0 | 23.2 | 3.2 | 4.05 | 4.99 | 1.39 | 2.05 |
| 3 | 12.6 | 0 | 16 | 2.4 | 4.07 | 4.98 | 1.85 | 1.96 |
| 4 | 10.2 | 0 | 35 | 3.6 | 4.23 | 4.37 | 0.347 | 4.55 |
| 5 | 10 | 0 | 35 | 4.2 | 4.23 | 4.08 | 0.355 | 3.67 |
| 6 | 10.6 | 0 | 35.2 | 6 | 4.47 | 4.61 | 0.937 | 3.57 |
| 7 | 10.8 | 0 | 17.4 | 2.6 | 4.76 | 4.68 | 1.32 | 1.88 |
| 8 | 10 | 0 | 35 | 5.2 | 4.24 | 4.36 | 0.195 | 3.96 |
| 9 | 10 | 0 | 25 | 2.4 | 4.8 | 4.77 | 0.565 | 3.21 |
| 10 | 10.8 | 0 | 27 | 3.6 | 4.97 | 4.98 | 1.21 | 2.38 |
| 11 | 10 | 0 | 16 | 2.4 | 4.23 | 4.08 | 0.355 | 3.67 |
| 12 | 10.2 | 0 | 35 | 3.6 | 4.02 | 4.77 | 0.41 | 4.89 |
| 13 | 9.8 | 0 | 35 | 5.2 | 4.51 | 4.37 | 0.276 | 4.34 |
| 14 | 12.2 | 0 | 35.2 | 6 | 4.23 | 4.62 | 1.19 | 2.31 |
| 15 | 10.6 | 0 | 35.2 | 7 | 4.52 | 4.91 | 1.16 | 4.27 |
| 16 | 10 | 0 | 35 | 4.8 | 4.27 | 4.37 | 0.212 | 3.85 |

(11) may be used to write the polynomials obtained for the numerator ($N_1$, $N_2$, $N_3$, $N_4$) and the denominator ($D_1$, $D_2$, $D_3$, $D_4$). These 8 Kharitonov polynomials are used to construct the 16 required Kharitonov plants. For the 7-state WT, the denominator, $D_i(s)$, and the numerator, $N_i(s)$, where $i = 1, 2, 3, 4$, have been determined and are shown in detail in Tables 1 and 2. Subsequently, Kharitonov's rectangles are formed to satisfy the zero-exclusion principle (Asadi, 2018) as shown in Figure 2. The robustly stabilizing PI controller is obtained by designing the acceptable region ($K_p$, $K_i$) as shown in Section 5.2.

In this paper, the primary aspect in the design of a PI controller (Figure 3) is to robustly stabilize (rotor rated speed, 42 rpm) an uncertain seven-state WT, applied with ±25% uncertainty on 21 elements of its system matrix. To achieve the robustly stabilizing acceptable ($K_p$, $K_i$) region shown in Figure 4, which is an intersection of all 16 plants, 150 iterations were executed in the simulations. The ($K_p$, $K_i$)-region is shown for all 16 plants collectively (Figure 4) and the sub-regions for all 16 plants individually (Figure 5). It is observed that any point in the 2-dimensional ($K_p$, $K_i$) region can robustly stabilize the uncertain WT effectively. But eventually, what matters is the minimization of time response specifications. Hence, the sub-region is extracted from the ($K_p$, $K_i$) region based on peak overshoots (<5%) and settling times (<5 s).

## *Settling time and % peak overshoot*

The minimum value and maximum value of both $K_p$ and $K_i$ in each sub-region were extracted and furnished in Table 3, which again presents the settling times and peak overshoot of each Kharitonov plant individually. These time response specifications are in accordance with Figure 6. It is observed that the 12$^{th}$ Plant controlled by gains (10.2, 0) has a minimum settling time of 4.02 s with a % peak overshoot of 0.41%. Similarly, two of the 16 plants numbered 5 and 11 which are controlled by different gains (35, 4.2) and (16, 2.4) respectively, achieved same settling times

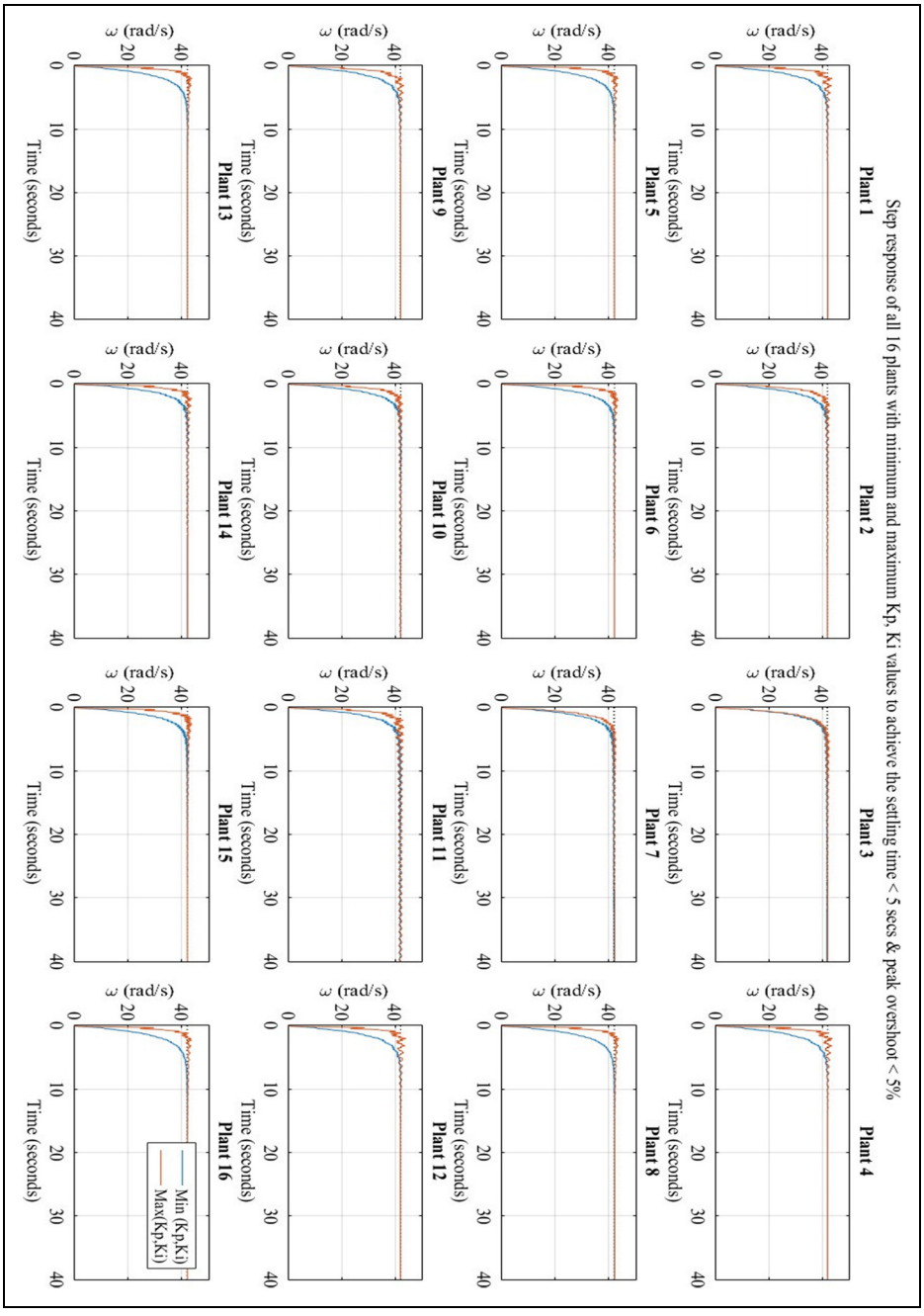


**Figure 6.** The step response of all 16 plants with the lowest and highest $K_p$, $K_i$ values to get the appropriate peak overshoot and settling time.

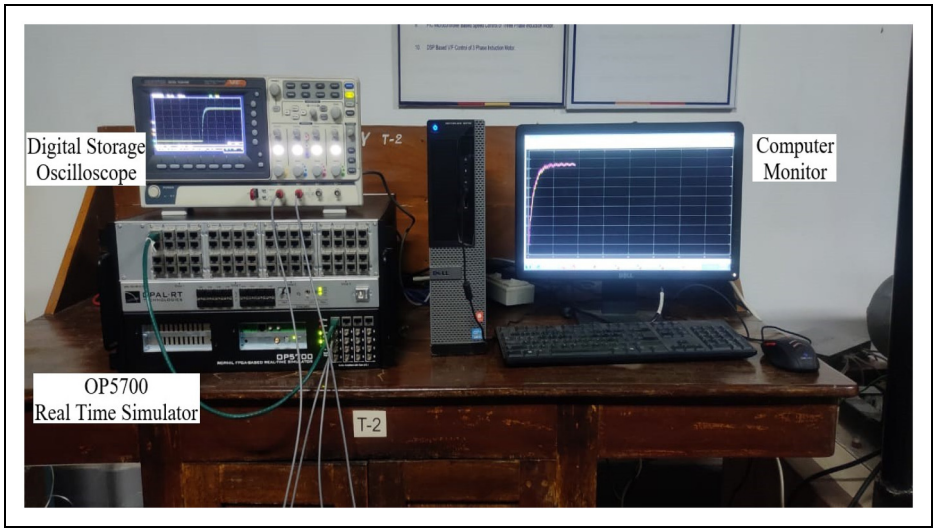


**Figure 7.** Set-up of real-time simulation.

(4.08 s minimum) and same % peak overshoot (3.67%) shown in the maximum ($K_p$, $K_i$) column of Table 3. The plant numbered 8 could achieve the lowest % peak overshoot (0.195%) that was controlled by gains (10, 0). Similarly, the plant numbered 12 has the maximum % peak overshoot (4.89%) that was controlled by gains (35, 3.6).

### *Real-time simulations of robust controllers for the 16-plant model of an uncertain wind turbine*

This paper also presents real-time simulation results of the designed robust controllers for an uncertain multi-input wind turbine. The real-time simulation set-up is shown in Figure 7. The real-time simulation software is completely compatible with the MATLAB/SIMULINK environment (Mohanty et al., 2018). The Simulink model is built, loaded, and executed by the real-time simulation software in the OPAL RT OP5700 Simulator. The rotor speed of 42 rpm is obtained for all 16 plants formed in section 4.1 in a real-time environment. The same two sets (minimum and maximum combinations given in Table 3) of controller gains were used to check for the robustness of the designed controllers in a real-time environment. Results of all 16 plants are shown in Figure 8, where it is observed that the desired specifications, namely, the settling times less than 5 s and peak overshoots less than 5%, are achieved, which validates the performance of all designed controllers in MATLAB shown in Figure 6.

## Conclusion

A multi-input WT with control input($\beta$) and wind disturbances is considered and subjected to $\pm$25% uncertainty. The system matrix has twenty-one elements to which this uncertainty value is applied. Kharitonov's 16-plant theorem approach is used to design the robustly stabilizing ($K_p$, $K_i$) region by forming Kharitonov's rectangles. In this case, any value of $K_p$ & $K_i$ in this area may robustly stabilize the wind turbine, i.e., regulate the rotor speed to its rated value of 42 rpm. A sub-region is also

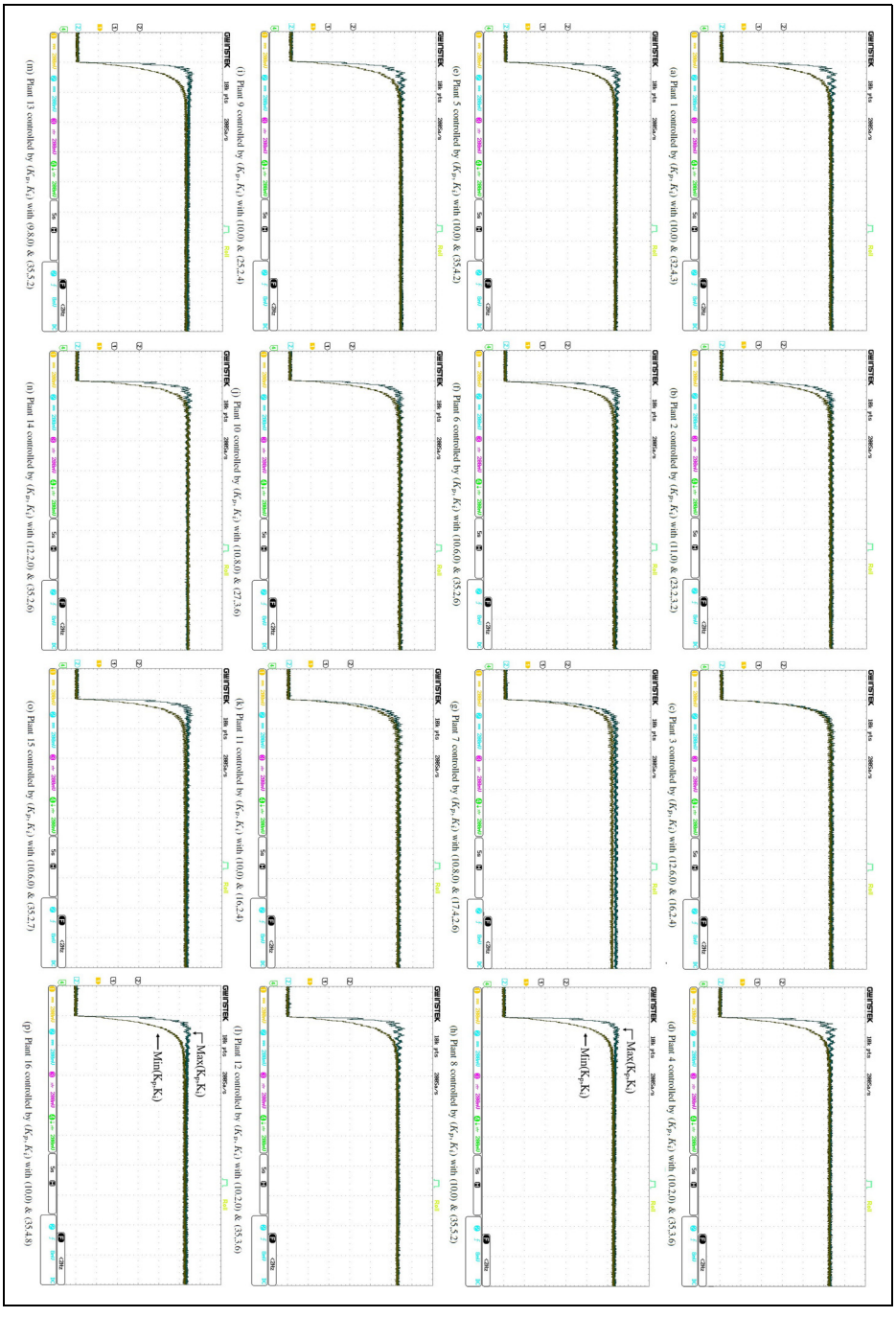


**Figure 8.** The real-time simulation results for controlling the rotor speed to 42 rpm rated value. Plants numbered 1 to 16 are shown in this figure.

formed for all the 16 plants individually to solely achieve the desired time response specifications, which are settling times less than 5 s and peak overshoots less than 5%. Eventually, the minimum and maximum values of ($K_p$, $K_i$) chosen from the sub-regions are found to strictly achieve the mentioned specifications, which validates the performance of robust controllers designed in MATLAB. To further evaluate the ad, validate the performances, real-time simulations made on the OPAL RT OP5700 simulator are also furnished.

## ORCID iDs

Daniel Eutyche Mbadjoun Wapet https://orcid.org/0000-0001-8682-5932
Mohamed Metwally Mahmoud https://orcid.org/0000-0002-2460-1850

## Authorship contribution

All authors have equally contributed to every facet of this research. Their joint efforts encompassed: Conceptualization; Data curation; Formal analysis; Investigation; Methodology; Project administration; Resources; Software; Supervision; Validation; Visualization; Roles/Writing—original draft; and Writing—review and editing.

## Funding

The authors received no financial support for the research, authorship, and/or publication of this article.

## Declaration of conflicting interests

The authors declared no potential conflicts of interest with respect to the research, authorship, and/or publication of this article.

## Data availability statement

Availability of data and materials Datasets used and/or analyzed during the current study are available from the corresponding author upon reasonable request.

## References

Adeoye O, Binzaid S and Attia J (2024) Performance of an omnidirectional wind energy harvesting system for low wind-speeds. In: 2024.

Aldin NAN, Abdellatif WSE, Elbarbary ZMS, et al. (2023) Robust speed controller for PMSG wind system based on harris hawks optimization via wind speed estimation: A real case study. *IEEE Access* 11: 5229–5943.

Apata O and Oyedokun DTO (2020) An overview of control techniques for wind turbine systems. *Scientific African* 10: e00566.

Asadi F (2018) Robust control of DC-DC converters: The Kharitonov's theorem approach with MATLAB® codes. *Synthesis Lectures on Power Electronics*. https://link.springer.com/book/10.1007/978-3-031-02503-7

Atia BS, Mahmoud MM, Elzein IM, et al. (2024) Applications of Kepler algorithm-based controller for DC chopper: Towards stabilizing wind driven PMSGs under nonstandard voltages. *Sustainability (Switzerland)* 16(7): 2952–2977.

Bahmani H, Bayat F and Golchin M (2020) Wind turbines power regulation using a low-complexity linear parameter varying-model predictive control approach. *Transactions of the Institute of Measurement and Control* 42(1): 81–93.

Bhattacharyya SP (2017) Robust control under parametric uncertainty: An overview and recent results. *Annual Reviews in Control* 44: 45–77.

Boudjemai H, Ahmed S, Mehdi E, et al. (2023a) Experimental analysis of a new low power wind turbine emulator using a DC machine and advanced method for Maximum wind power capture. *IEEE Access* 11: 92225–92241.

Boudjemai H, Ardjoun SA, Chafouk H, et al. (2023b) Application of a novel synergetic control for optimal power extraction of a small-scale wind generation system with variable loads and wind speeds. *Symmetry* 15(2): 92225–92241.

Boudjemai H, Ardjoun SAEM, Chafouk H, et al. (2025) Design, simulation, and experimental validation of a new fuzzy logic-based maximal power point tracking strategy for low power wind turbines. *International Journal of Fuzzy Systems* 5(1): 296–310.

Boutabba T, Benlaloui I, Mechnane F, et al. (2025) Design of a small wind turbine emulator for testing power converters using dSPACE 1104. *International Journal of Robotics and Control Systems* 5(2): 698–712.

Cascianelli S, Astolfi D, Castellani F, et al. (2022) Wind turbine power curve monitoring based on environmental and operational data. *IEEE Transactions on Industrial Informatics* 18(8): 5209–5218.

Chishti F, Murshid S and Singh B (2020) Robust normalized mixed-norm adaptive control scheme for PQ improvement at PCC of a remotely located wind-solar PV-BES microgrid. *IEEE Transactions on Industrial Informatics* 16(3): 1708–1721.

Chu M and Chu J (2018) Graphical robust PID tuning based on uncertain systems for disturbance rejection satisfying multiple objectives. *International Journal of Control, Automation and Systems* 16(5): 2033–2042.

El Beshbichi O, Xing Y and Chen Ong M (2023) Modelica-AeroDyn: Development, benchmark, and application of a comprehensive object-oriented tool for dynamic analysis of non-conventional horizontal-axis floating wind turbines. *Wind Energy* 26(6): 538–572.

Errouissi R, Al-Durra A and Debouza M (2018) A novel design of PI current controller for PMSG-based wind turbine considering transient performance specifications and control saturation. *IEEE Transactions on Industrial Electronics* 65(11): 8624–8634.

Fayz A, Ahmed A, Elzein IM, et al. (2025) Optimal controller design of crowbar system for DFIG-based WT : Applications of gravitational search algorithm. *Buletin Ilmiah Sarjana Teknik Elektro* 7(2): 122–136.

Habibi H, Rahimi Nohooji H and Howard I (2018) Adaptive PID control of wind turbines for power regulation with unknown control direction and actuator faults. *IEEE Access* 6: 37464–37479.

Hamoodi SA, Hameed FI and Hamoodi AN (2020) Pitch angle control of wind turbine using adaptive fuzzy-PID controller. *EAI Endorsed Transactions on Energy Web* 7(28): e15.

Huang SL, Chen JF, Liang TJ, et al. (2020) Prediction of salt contamination in the rotating blade of wind turbine under lightning strike occurrence using fuzzy c-means and kmeans clustering approaches. *IET Science, Measurement and Technology* 14(1): 91–97.

Isbeih YJ, El Moursi MS, Xiao W, et al. (2019) H∞ mixed-sensitivity robust control design for damping low-frequency oscillations with DFIG wind power generation. *IET Generation, Transmission and Distribution* 13(19): 4274–4286.

Jafari A and Shahgholian G (2017) Analysis and simulation of a sliding mode controller for mechanical part of a doubly-fed induction generator-based wind turbine. *IET Generation, Transmission and Distribution* 11(10): 2677–2688.

Kheshti M, Ding L, Bao W, et al. (2020) Toward intelligent inertial frequency participation of wind farms for the grid frequency control. *IEEE Transactions on Industrial Informatics* 16(11): 6772–6786.

Liu X, Han Y and Wang C (2017) Second-order sliding mode control for power optimisation of DFIG-based variable speed wind turbine. *IET Renewable Power Generation* 11(2): 408–418.

Mahmoud MM, Atia BS, Abdelaziz AY, et al. (2022a) Dynamic performance assessment of PMSG and DFIG-based WECS with the support of manta ray foraging optimizer considering MPPT, pitch control, and FRT capability issues. *Processes* 10(12): 2723–2751.

Mahmoud MM, Atia BS, Esmail YM, et al. (2023a) Evaluation and comparison of different methods for improving fault ride-through capability in grid-tied permanent magnet synchronous wind generators. *International Transactions on Electrical Energy Systems* 2023: 1–22.

Mahmoud MM, Khalid Ratib M, Aly MM, et al. (2022b) Wind-driven permanent magnet synchronous generators connected to a power grid: Existing perspective and future aspects. *Wind Engineering* 46(1): 189–199.

Mahmoud MM, Salama HS, Bajaj M, et al. (2023b) Integration of wind systems with SVC and STATCOM during Various events to achieve FRT capability and voltage stability: Towards the reliability of modern power systems. *International Journal of Energy Research* 2023: 1–28.

Matušů R (2011) Calculation of all stabilizing PI and PID controllers. *International Journal of Mathematics and Computers in Simulation* 5(3): 224–231.

Menzri F, Boutabba T, Benlaloui I, et al. (2024) Applications of novel combined controllers for optimizing grid-connected hybrid renewable energy systems. *Sustainability (Switzerland)* 16(16): 6825–6849.

Metwally Mahmoud M (2023) Improved current control loops in wind side converter with the support of wild horse optimizer for enhancing the dynamic performance of PMSG-based wind generation system. *International Journal of Modelling and Simulation* 43(6): 952–966.

Mohanty A, Viswavandya M, Ray PK, et al. (2018) Literature survey on OPAL-RT technologies with advance features and Industrial applications. In: 1st International Conference on Advanced Research in Engineering Sciences, ARES 2018, 2018.

Naghdalian S, Amraee T, Kamali S, et al. (2020) Stochastic network-constrained unit commitment to determine flexible ramp reserve for handling wind power and demand uncertainties. *IEEE Transactions on Industrial Informatics* 16(7): 4580–4591.

Petkov PH, Slavov TN and Kralev JK (2018) *Design of Embedded Robust Control Systems Using MATLAB®/Simulink®*.

Rigatos G and Siano P (2011) Design of robust electric power system stabilizers using Kharitonov's theorem. *Mathematics and Computers in Simulation* 82(1): 181–191.

Saidi Y, Mezouar A, Miloud Y, et al. (2021) Adaptive control of wind turbine generators for power capture optimization by using integral backstepping approach during partial-load operation. *Journal of Control, Automation and Electrical Systems* 32(4): 1041–1052.

Salem A, Abu-Siada A and Islam S (2017) Improved condition monitoring technique for wind turbine gearbox and shaft stress detection. *IET Science, Measurement and Technology* 11(4): 431–437.

Soliman MA, Hasanien HM, Azazi HZ, et al. (2019) An adaptive fuzzy logic control strategy for performance enhancement of a grid-connected PMSG-based wind turbine. *IEEE Transactions on Industrial Informatics* 15(6): 3163–3173.

Toulabi M, Dobakhshari AS and Ranjbar AM (2018) Optimal robust first-order frequency controller design for DFIG-based wind farm utilising 16-plant theorem. *IET Renewable Power Generation* 12(3): 298–310.

Vo HH (2018) Fast stability analysis for proportional-integral controller in interval systems. *Journal of Advanced Engineering and Computation* 2(2): 111.

Wang X, Gao W, Gao T, et al. (2018) Robust model reference adaptive control design for wind turbine speed regulation simulated by using FAST. *Journal of Energy Engineering* 144(2): 04018007.

Wright AD and Balas MJ (2003) Design of state-space-based control algorithms for wind turbine speed regulation. *Journal of Solar Energy Engineering, Transactions of the ASME* 125(4): 386–395.